

Creating a Pipeline to Search for Dwarf Nova Eruptions in Globular Cluster M15

IMAN BEHBEHANI,¹

(705 THESIS PAPER)

M. SHARA,² D. ZUREK,² E. GLIKMAN,¹

¹*Middlebury College Department of Physics*

14 Old Chapel Road

Middlebury, VT 05753, USA

²*Department of Astrophysics, American Museum of Natural History*

New York, NY 10024

ABSTRACT

The globular cluster Messier 15 is known for its high incidence of variable star systems, yet contains only two known dwarf nova candidates. The *SWIFT* telescope has produced a wealth of archival ultraviolet images, where short wavelength-bright dwarf nova eruptions should be detectable. This study reports on a thorough investigation of unsearched *SWIFT* telescope images of M15, testing whether we can fill in a gap in our understanding of variables in this cluster. I searched 10 epochs of *SWIFT* telescope images for variables by coding a pipeline to create difference images to track variable stars over time. I used patterns made by variable stars during subtraction to identify and produce a catalog of 169 variable star candidates to be compared with data of known transients in M15. This study marks the first *SWIFT* ultraviolet search for dwarf novae in M15, and builds a pipeline to efficiently search *SWIFT* data of any globular cluster for dwarf novae.

Keywords: Dwarf Novae (251) — Ultraviolet astronomy(1736) — Globular star clusters(656)

1. INTRODUCTION

Cataclysmic variable stars (CVs) are binary star systems composed of a white dwarf and a main sequence star. Most stars in the galaxy are “main sequence,” and fuse hydrogen into helium to produce energy in their cores. White dwarf stars are the end of life remnants of main sequence stars $< 8M_{\odot}$. If a white dwarf has a close companion, it accretes material through an accretion disk, illustrated in Figure 1. These companions become attached to the white dwarf via two- or three-body tidal capture, in which two stars become gravitationally bound, or two stars in a three-body system latch onto each other (Fabian et al. 1975; Michael & Shara 2021). These interactions are more likely to occur in Globular Clusters (GCs) because of the higher density of stars. 1 in every 10,000 stars near the Sun is a CV, with a predicted higher (10-100X) prevalence in GCs.

Globular clusters are densely packed, gravitationally bound groups of tens of thousands to millions of stars, typically 10 to 13 billion years old (Vandenbergh et al. 1996). Messier 15, heretofore referred to as “M15,” is one of the oldest GCs in the Milky Way at 13.2 Gyr

(McNamara et al. 2004). At a distance of 10.3kpc away (van den Bosch et al. 2006), M15 is close enough that we are avoiding poor star resolution likely at greater distances (Kayal & Benacquista 2013). The median core radius of globular clusters is $\sim 1\text{pc}$, with a density of $70M_{\odot}\text{pc}^{-3}$ (Marx & Pfau 1992). M15, which has likely undergone core collapse, is extremely dense at its core, $r_c \approx 0.07'$, $\rho_c \approx 7 \times 10^6 M_{\odot}\text{pc}^{-3}$ (van den Bosch et al. 2006).

CVs can generally be categorized as magnetic and non-magnetic. Magnetic CVs typically do not have accretion disks around the white dwarf, while non-magnetic CVs always will. The accretion disk is a gravitationally bound, rotating disk of accumulated material from the companion star. The disk instability model (Lasota 2001) details imbalances causing material from the accretion disk to be transferred to the white dwarf’s surface in periodic bursts, during which the system’s brightness temporarily increases significantly. As ionized hydrogen is accreted from the main sequence star, it becomes more and more dense, and consequently more viscous, unable to rotate fast enough to resist gravita-

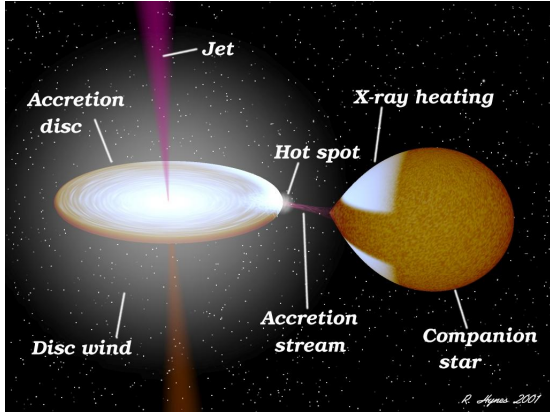


Figure 1. Model of the transfer of mass from the companion star (right) to the white dwarf (left) Zurek et al. (2016).

tional collapse. The disk falls onto the white dwarf, releasing energy as heat. This outburst is known as a dwarf nova.

This study uses archive data from the *Niel Gehrels Swift Observatory's SWIFT* telescope. *SWIFT* was designed with the intention of studying Gamma Ray bursts (GRBs), which present as sudden flashes of gamma ray light. Designed around the short and sudden nature of these outbursts, *SWIFT*'s Burst Alert Telescope (BAT) will detect GRBs and relay their positions to the ground. In under 90 seconds, *SWIFT* will “swiftly” orient its X-Ray and UV/optical telescopes (UVOT) toward the burst location to capture the afterglow, resulting in a large database of UV images¹. I am using images specifically from UVOT. UVOT has a 17' x 17' field of view, with UV filters *UVW1*, *UVM2* and *UVW2* (Modiano et al. 2022). I focused on the *UVM2* filter, as it has the smallest “red leak” optical contamination, between *UVW1*, *UVM2*, and *UVW2* (Siegel et al. 2015). Figure 2 shows the effective area (basically detection efficiency) in cm^2 versus wavelength in Angstrom of all seven of UVOT's broadband filters. The *UVW1* and *UVW2* filters have extended red tails, meaning the flux they measure will include a contribution from the source's optical flux as well as UV³. For this study, this means that some additional non-CV sources would be included. Thus, *UVM2* is the preferred filter to start with. *UVW1* and *UVW2* can still be used for future searches, or to build color magnitude diagrams of the sources detected.

Most stars, our sun included, occupy an area of the color magnitude diagram (also called the Hertzsprung-

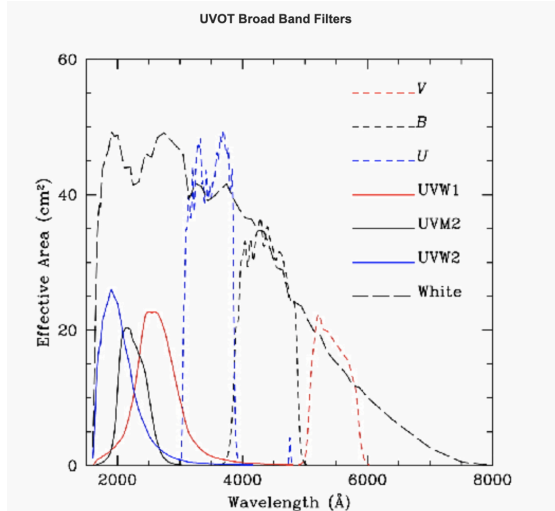


Figure 2. Effective area curves of all seven broadband filters of *SWIFT*'s UVOT telescope via NASA. Notice the red leak in *UVW1* and *UVW2*.

Russell (HR) diagram) called the main sequence, with the defining characteristic of burning core hydrogen to release energy. As these stars evolve and run out of core hydrogen, they turn off the main sequence towards the red giant branch, fusing hydrogen in a shell around their now-inert helium cores, and increasing their luminosities up to a thousandfold. An HR diagram with placements of these stars can be seen in Figure 3. Since CVs are composed of a white dwarf and main sequence star, CV candidates occupy the space between WD and the main sequence groups on the HR diagram in Figure 3. GCs are mostly populated by old main sequence, red stars, all of which are fainter than the sun. However, the luminosities of the GCs are dominated by the ≈ 1 percent of stars that are red giants. Evolved main sequence stars, red giants, have high luminosities around 100 to $1000 L_\odot$, which make them extremely prominent in GCs. Red giants can be an obstacle when searching for dwarf novae in optical filters.

Dieball et al. (2007) used *HST* images to make a UV color magnitude diagram of M15's core shown in Figure 4. Note UV color magnitude diagrams do not show the standard HR diagram group patterns as Figure 3, as the y axis shows its magnitude in the UV rather than optical. However, the magnitude difference between the far and near UV filters of each star is consistent. This is a proxy for temperature, with larger values cooler and lower values hotter. Notice the concentration of sources in the bottom right corner of Figure 4. This is the red giant and main sequence group, cool stars which are faint in the UV. This indicates that most of the light from these stars is not in the UV. Further, dwarf novae emit predominately at shorter wavelengths due to the

¹ swift.gsfc.nasa.gov/about_swift/

² swift.gsfc.nasa.gov/about_swift/uvot_desc.html

³ swift.gsfc.nasa.gov/analysis/uvot_digest/redleak.html

high temperature of the eruption and WDs. Short wavelength filters, including *SWIFT*'s UVOT, are therefore preferred for dwarf nova studies.

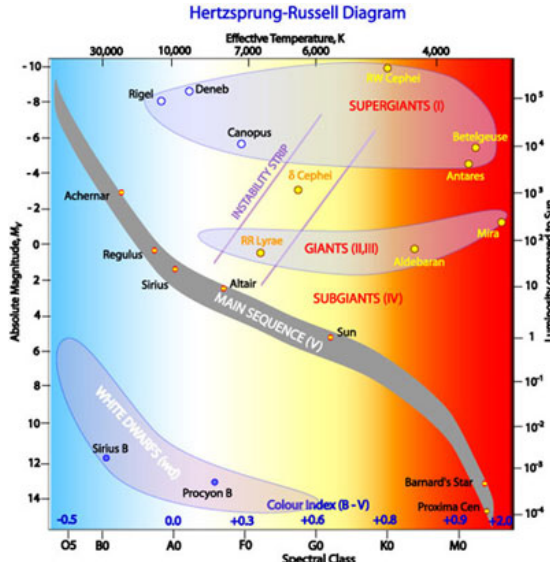


Figure 3. Standard HR Diagram (R. Hollow, CSIRO) depicting the relationship between magnitude and temperature for different stellar groups. Note the location of the main sequence and white dwarfs. CVs will be between the two (R. Hollow, CSIRO).

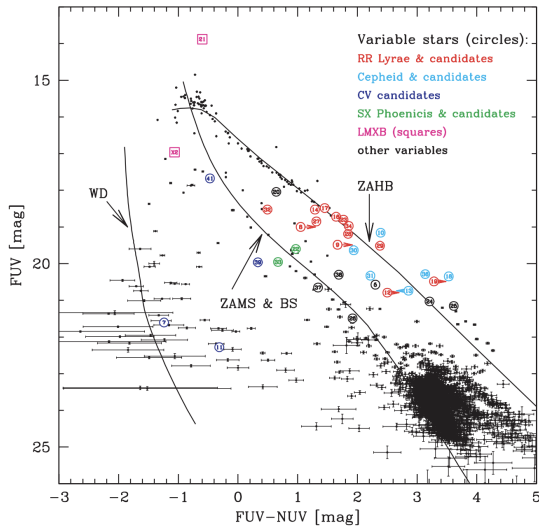


Figure 4. Ultraviolet HR Diagram of M15 produced by Dieball et al. (2007) showing the faintness of red and main sequence stars in the ultraviolet.

M15 has about 204 variable stars known, 149 of which are RR Lyrae (Dieball et al. 2007). RR Lyrae undergo rapid, pulsating changes in luminosity. To ensure the

transients detected in this study are not RR Lyrae or other known variables, their coordinates will be cross checked using the RR Lyrae catalog by Siegel et al. (2015) before confirming any candidates as DN.

M15 has not been thoroughly studied for DN. We only know of the two erupting CVs that Shara et al. (2004) and Charles et al. (2002) have found in *HST* data. Dieball et al. (2007) used an estimate for capture rate in GC cores using core density and radius, $\Gamma \propto \rho_c^{1.5} r_c^2$ (Heinke et al. 2003) for about ≈ 200 CVs in M15. This estimate is comparable to Di Stefano & Rapaport (1994)'s calculation for ≈ 190 tidal capture CVs in globular cluster 47 Tucanae. Both estimates are lower limits, as they exclude CVs formed by three-body tidal capture and aged CVs too faint for detection. As these are only two known CVs in M15, this paper intends to clarify this gap between tidal capture theory and confirmed data. This study will provide the first *SWIFT* DN search of M15 in the ultraviolet.

2. EXPERIMENTAL SETUP

2.1. Differencing

A difference image is the subtraction of two images, returning an output image that makes variable stars easy to identify. This methodology is ideal for comparing images taken at different times (epochs). Images in python can be depicted as 2-D numpy arrays, each index representing the brightness of the respective pixel. A difference image can be generated by aligning and subtracting the two image arrays from each other, thus subtracting the values of each pixel. See the code reproduced in Appendix A. The distinct pattern between unchanged background stars and dwarf novae can be seen in Figure 5. In this difference image developed for a dwarf nova in GC 47 Tucanae, the centered star is erupting, while its surroundings stay constant. The light and dark pattern on surrounding sources has been referenced by Modiano et al. (2022) as occurring in non-variable stars as a consequence of the subtraction process with either different PSFs or imperfect alignment. I will be nicknaming this as the “onigiri test” for the resemblance to the Japanese rice dish. I am using this pattern as an aide to rule out non-variable stars, focusing on sources not displaying this pattern, thus passing the onigiri test. If a star passes the onigiri test, it is “fully subtracted,” and will be added to my catalog of variable star candidates.

These images vary in exposure time. To avoid skewing the difference with an additional brightness difference, I scaled the brightness by dividing the image's numpy array by its exposure time. This use of ratios allows corresponding pixels to be in the proper brightness scale of counts per second. *SWIFT* images are generally aligned

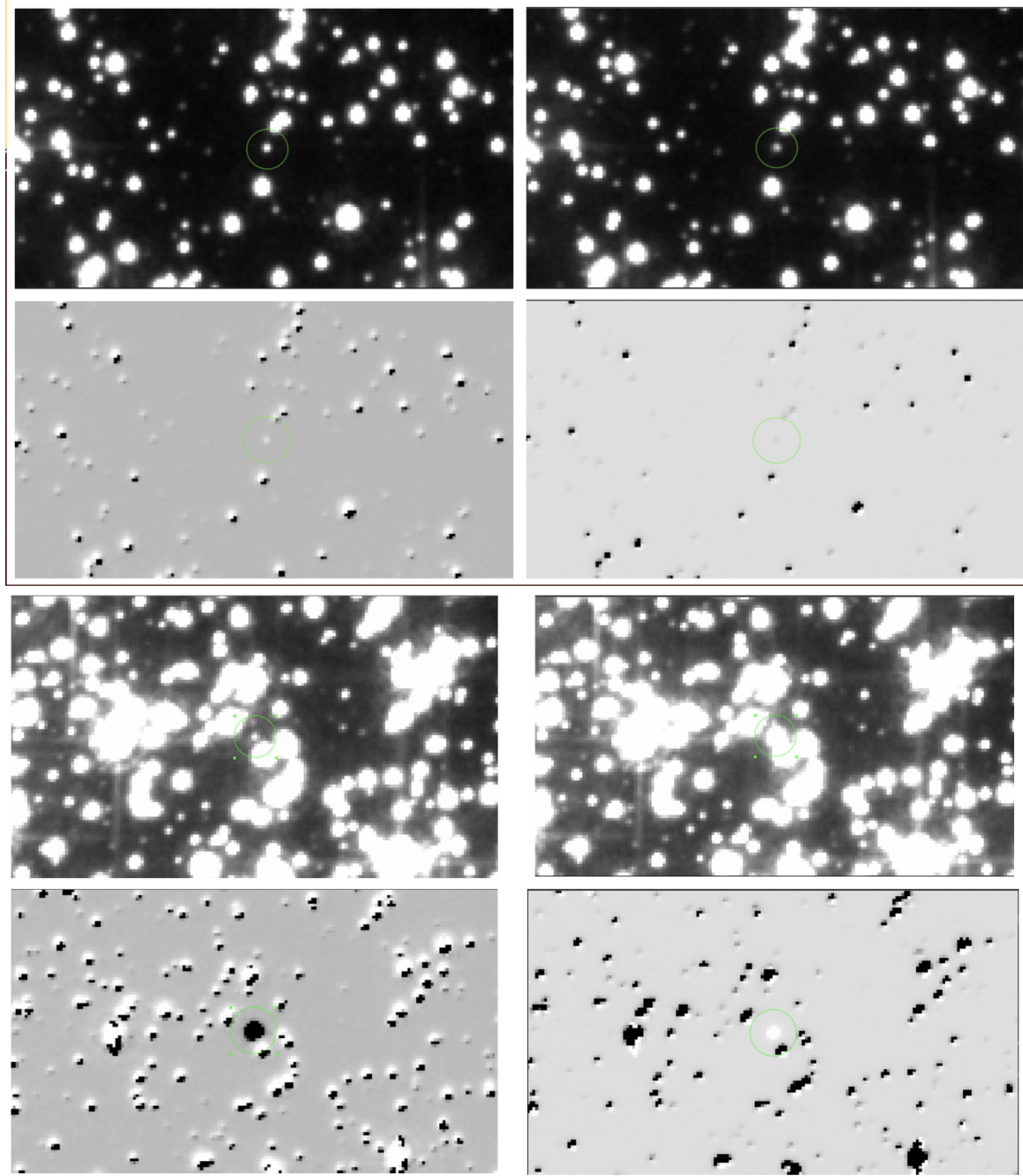


Figure 5. Difference images for dwarf nova candidates using *HST* images of 47 Tucanae produced in Behbehani et al. (2022). A faint dwarf nova found is shown in the top panel, and an eruption found by Rivera Sandoval et al. (2018) is shown in the bottom panel. For each panel, the top row has the epoch 1 and epoch 2 (right to left), with difference images in the bottom row (left is epoch 2 subtracted from 1, and right epoch 1 subtracted from 2).

rotationally, but may have an xy shift or variation in size. To align epochs for a proper subtraction, I used *Cutout2D* in astropy to pick a center star, and crop epochs around it. This way, the images I subtracted were calibrated around the same centroid, and cropped to dimensions that included as much of each epoch as possible.

After the images were created, I scanned the difference image for fully subtracted sources, adding their coordinates to a catalog to be compared to existing records of known transients in M15, especially RR Lyrae, in future research.

2.2. Image Selection

As described in the introduction, a key identifier of erupting dwarf novae is a large increase in brightness (typically 10-100x) for a period of 3-10 days. I searched for stars with large brightness increases by comparing stars between *SWIFT* epochs that fit the parameters outlined below. I selected five image pairs from *SWIFT*'s public online database. It is essential that images in a brightness comparison have similar exposures and the same filter. Otherwise, it may appear as though constant sources have varied. Although I scaled the pixels for exposure before differencing, I made sure to pick epochs with exposures within ≈ 25 percent of each other so stars of similar brightnesses would be present in each image. Longer exposure images included fainter stars, and were thus preferred to make my search more thorough. Lastly, all image pairs must be taken at least two weeks apart to allow for potential dwarf nova eruptions to fully begin or subside by the subsequent image. The resulting set of 10 images are shown in Table 1. Images were taken between 2013 and 2015, with exposure times from 245s to 1086s.

Epoch	Obs ID	Date	Exposure (s)
1	84193001	10/16/2014	286.936
2	84193002	1/6/2015	245.835
3	91683006	5/22/2013	969.32
4	91683009	6/15/2013	949.742
5	91683019	8/2/2013	1086.662
6	91683027	9/3/2013	1006.903
7	91683035	10/5/2013	946.832
8	91683042	11/18/2013	945.768
9	91683045	12/12/2013	1050.404
10	91683005	5/14/2013	1058.363

Table 1. List of images studied with date and exposure in the *UVM2* filter, separated by pairs compared.

3. RESULTS

My search resulted in a catalog of 169 transients pending further review. I successfully created 5 difference images for analysis. Using the Space Telescope Science Institute's archive ⁴, I set a search for M15 images in the *UVM2* filter with exposures over 100s. I marked and downloaded the datasets I picked in Table 1, converted the filter coadded "sk" images from img to fits files by manually changing the file name ending. FITS files are standard astronomical data files containing in-

formation about the images and how it was taken. I then entered each pair into my difference code, provided in Appendix A. I aligned the images about a shared center and subtracted them.

I was able to line the images up in the astronomy image software ds9, and compare stars that passed the onigiri test. Figure 6 show side-by-sides of the pair cutouts and their difference images, with the circles marking the candidates I had found in my first round of searching. I did two rounds of searches; as I analyzed more epochs, I became better at recognizing variables and scaling images to resolve more of the core. I did a second round of searching after gaining that experience, and found 40 additional candidates. This project is subject to human error in recognition; meticulous image review was essential.

I found a total of 169 candidates across all epochs, with 42 in pair 1, 30 in pair 2, 23 in pair 3, 42 in pair 4, and 32 in pair 5. A full list of candidates with their locations is in Appendix B. These candidates are not unique; many repeat, and are therefore likely RR Lyrae pulsating over a short period captured by multiple epochs. This is an analytical step to be taken alongside further data reduction. An animation depicting the candidates across epochs can be seen at [this link](#). The cyan circles indicate candidates in the catalog; the large portion that recur throughout epochs are most likely RR Lyrae.

4. CONCLUSION

This project built a catalog of variable stars across 10 *SWIFT* telescope images of M15, building the foundation for a deeper analysis of the GC's stellar composition. All 10 epochs were sourced from the Space Telescope Science Institute online data archive, making this study accessible and reproducible. I used epochs from *SWIFT*'s lowest red leak UV filter *UVM2* with exposure times from 200 to 1100 seconds. After producing difference images in python and comparing them to the original images, I found a total of 169 variables.

The large majority of these brightenings are likely those of RR Lyrae stars. On the instability strip of the Hertzsprung-Russel diagram (Figure 3), RR Lyrae pulse as the opacity of their ionized helium varies with temperature. This change in temperature manifests as a +3 magnitude difference in the UV, while only a +0.5 magnitude change in the optical. Thus, 149 known RR Lyrae in M15 mean there are 149 sources with considerable magnitude changes flashing every day in the UV data of M15. Consequently, RR Lyrae are a significant contaminant in this study. RR Lyrae can be seen on the instability strip of the HR Diagram in Figure 7. These RR Lyra star brightenings exhibit periods of several hours

⁴ archive.stsci.edu/swiftuvot/

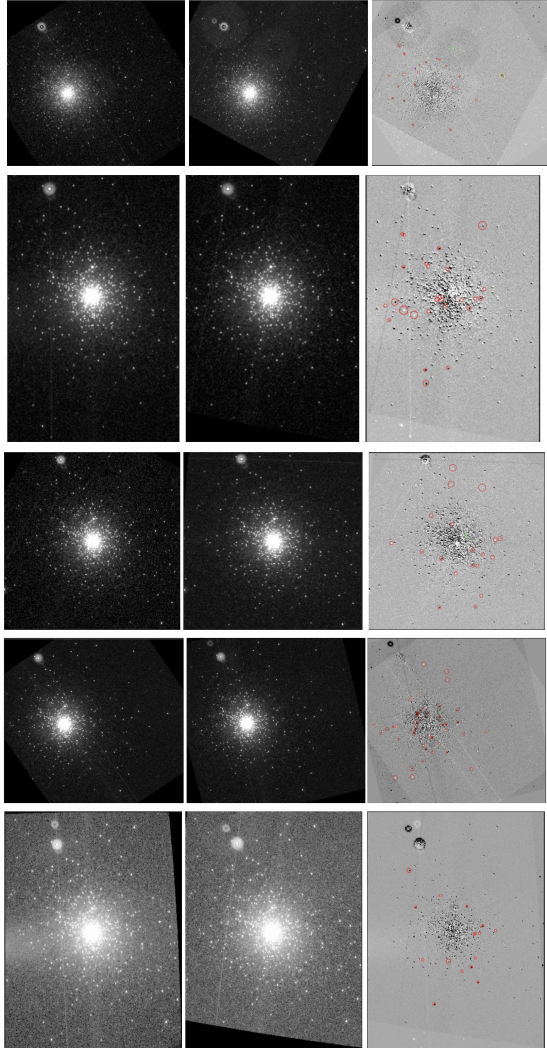


Figure 6. All 5 *SWIFT* epoch pairs (1-5 top to bottom) beside the subtraction image produced between them (left to right). The red circles in the difference image mark different variable candidates.

to one day. Due to their short periods and high visibility in the UV, it is likely that many pulsing RR Lyrae were found in this search. CVs are located between the main sequence (labeled ZAMS for Zero Age Main Sequence) and the white dwarfs (bottom left) of Figure 7. Using the magnitudes of candidates across different filters to plot them on an HR Diagram is another way to determine if it's a dwarf nova, as RR Lyrae and CVs occupy distinct places on this diagram. As this candidate list is reduced to skip repeat candidates, I will make color magnitude diagrams to infer the likely identities of the candidates.

Another complication of this study was stellar resolution at the M15's core. *SWIFT* has an angular resolution of $18''$, and therefore cannot distinguish individual

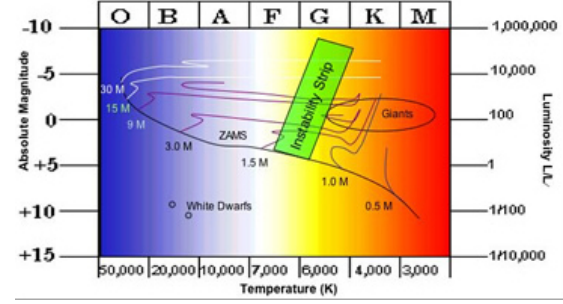


Figure 7. Diagram showing the location of the instability strip on the HR Diagram, home to variable stars RR Lyrae, Cepheid variable, W Virginis and ZZ Ceti(Swinburne University).

stars close to M15's dense core. As a binary star system with a white dwarf, the total mass of a CV is about double that of main sequence stars in GCs; their higher mass will draw CVs towards the cores of globular clusters. This means we are unlikely to see CVs in M15's core with *SWIFT*. Other GCs with less dense cores are likely better targets for ongoing searches for erupting DNs in GCs.

Although most of my 169 sources are likely RR Lyrae, this catalog provides the necessary foundation to find dwarf nova eruptions in M15, if there are any to be discovered. The confirmation of dwarf nova eruptions will provide a significant test of tidal capture theory's prediction for the rate of CVs and DN in globular clusters.

SWIFT has a rich database with additional clusters worth exploring. Originally written for *HST* data of GC 47 Tucanae, my code was designed to be adaptable to different datasets. Future research will expand the application to other globular clusters, including but not limited to M80 (NGC 6093), NGC 6752, and NGC 6397. This study shows that this code is effective in finding variables and can be applied to a broad range of globular clusters' images from different telescopes. While further analysis is required to interpret this catalog, I am able to confidently say that I have built a methodology that can efficiently search for dwarf novae in any globular cluster.

5. ACKNOWLEDGEMENTS

I would like to thank my advisors at Middlebury College and the American Museum of Natural History for their guidance throughout this project. Specifically, I'd like to thank Professor Eilat Glikman for her thorough supervision of this project, allowing me to research externally. Michael Shara and David Zurek were extremely generous in their mentorship, and I am grateful for the research experience they have extended me.

Facilities: SWIFT(UVOT)

Software: astropy (Astropy Collaboration et al. 2018)

REFERENCES

- Astropy Collaboration, Price-Whelan, A. M., Sipőcz, B. M., et al. 2018, AJ, 156, 123, doi: [10.3847/1538-3881/aabc4f](https://doi.org/10.3847/1538-3881/aabc4f)
- Behbehani, I., Shara, M., & Zurek, D. 2022
- Charles, P. A., Clarkson, W. I., & van Zyl, L. 2002, NewA, 7, 21, doi: [10.1016/S1384-1076\(01\)00087-2](https://doi.org/10.1016/S1384-1076(01)00087-2)
- Di Stefano, R., & Rappaport, S. 1994, ApJ, 423, 274, doi: [10.1086/173805](https://doi.org/10.1086/173805)
- Dieball, A., Knigge, C., Zurek, D. R., et al. 2007, ApJ, 670, 379, doi: [10.1086/522103](https://doi.org/10.1086/522103)
- Fabian, A. C., Pringle, J. E., & Rees, M. J. 1975, MNRAS, 172, 15, doi: [10.1093/mnras/172.1.15P](https://doi.org/10.1093/mnras/172.1.15P)
- Heinke, C. O., Grindlay, J. E., Lugger, P. M., et al. 2003, ApJ, 598, 501, doi: [10.1086/378885](https://doi.org/10.1086/378885)
- Kayal, K., & Benacquista, M. 2013, in American Astronomical Society Meeting Abstracts, Vol. 221, American Astronomical Society Meeting Abstracts #221, 354.10
- Lasota, J.-P. 2001, NewAR, 45, 449, doi: [10.1016/S1387-6473\(01\)00112-9](https://doi.org/10.1016/S1387-6473(01)00112-9)
- Marx, S., & Pfau, W. 1992, Astrophotography with the Schmidt Telescope
- McNamara, B. J., Harrison, T. E., & Baumgardt, H. 2004, ApJ, 602, 264, doi: [10.1086/380905](https://doi.org/10.1086/380905)
- Michaely, E., & Shara, M. M. 2021, MNRAS, 502, 4540, doi: [10.1093/mnras/stab339](https://doi.org/10.1093/mnras/stab339)
- Modiano, D., Wijnands, R., Parikh, A., et al. 2022, A&A, 663, A5, doi: [10.1051/0004-6361/202142997](https://doi.org/10.1051/0004-6361/202142997)
- Rivera Sandoval, L. E., van den Berg, M., Heinkel, C. O., et al. 2018, MNRAS, 475, 4841, doi: [10.1093/mnras/sty058](https://doi.org/10.1093/mnras/sty058)
- Shara, M. M., Hinkley, S., Zurek, D. R., Knigge, C., & Bond, H. E. 2004, AJ, 128, 2847, doi: [10.1086/425631](https://doi.org/10.1086/425631)
- Siegel, M. H., Porterfield, B. L., Balzer, B. G., & Hagen, L. M. Z. 2015, VizieR Online Data Catalog, J/AJ/150/129
- van den Bosch, R., de Zeeuw, T., Gebhardt, K., Noyola, E., & van de Ven, G. 2006, ApJ, 641, 852, doi: [10.1086/500644](https://doi.org/10.1086/500644)
- Vandenbergh, D. A., Bolte, M., & Stetson, P. B. 1996, ARA&A, 34, 461, doi: [10.1146/annurev.astro.34.1.461](https://doi.org/10.1146/annurev.astro.34.1.461)
- Zurek, D. R., Knigge, C., Maccarone, T. J., et al. 2016, Monthly Notices of the Royal Astronomical Society, 460, 3660, doi: [10.1093/mnras/stw1190](https://doi.org/10.1093/mnras/stw1190)

APPENDIX

A. APPENDIX A: CODE

```
"""
Function to align a fits image, then create subtraction image

Date: 07/12/22
Author: Iman Behbehani
"""

import astropy

from astropy.io import fits
from astropy import wcs
from astropy.nddata import Cutout2D
from astropy import units as u
import numpy as np
import matplotlib.pyplot as plt
import astropy.io.fits as fits
from astropy.wcs import WCS
from astropy.visualization import simple_norm

import astroalign as aa

from astropy.coordinates import SkyCoord # High-level coordinates
from astropy.coordinates import ICRS, Galactic, FK4, FK5 # Low-level frames
from astropy.coordinates import Angle, Latitude, Longitude # Angles

import cv2
import imutils

# Let's Subtract <3

# set image 1, image 2

# image 1
hdu1010 = fits.open("/Users/imam/Documents/Midd_Coursework/Fall_2022/704/amnh/swiftuvot4/epoch1.fits",
mode = 'update')
hdu1010[1].header['EXTNAME'] = 'SCI'
hdu1010[1].header['EXTVER'] = 1
data1 = hdu1010[1].data #this is already a numpy.ndarray
header10 = hdu1010[0].header
header11 = hdu1010[1].header

# image 2
hdu3010 = fits.open("/Users/imam/Documents/Midd_Coursework/Fall_2022/704/amnh/swiftuvot4/epoch2.fits",
mode = 'update')
hdu3010[1].header['EXTNAME'] = 'SCI'
hdu3010[1].header['EXTVER'] = 1
```

```

data2 = hdu3010[1].data
header20 = hdu3010[0].header
header21 = hdu3010[1].header

data = np.array(data1)

#making backup. mapping 1 onto 2
hdu1010a = hdu1010
data1a = hdu1010[1].data
header10a = hdu1010[0].header
header11a = hdu1010[1].header

hdu3010a = hdu3010
data2a = hdu3010[1].data
header20a = hdu3010[0].header
header21a = hdu3010[1].header

### finding and scaling exposures

header11['TELAPSE']
exp = header11["TELAPSE"]
data11a = data1a/exp

header21['TELAPSE']
exp2 = header21["TELAPSE"]
data22a = data2/exp2

# CUTOUT AND DIFFERENCE
here I make crop the input images around a shared star. this aligns them with the same dimensions

def cutout (x, y, data, hdu, filename):

    #center of cutout area coordinates
    xcoord = x
    ycoord = y

    #size of cutout image
    xsize = 1000
    ysize = 1000

    #cutout function (see astropy.nddata for documentation)
    cutout = Cutout2D(data, (xcoord,ycoord),(ysize,xsize))

    #Show our new image
    norm = simple_norm(cutout.data, 'sqrt', percent=98.1) #linear, log, sqrt

    plt.imshow(cutout.data, norm=norm, origin='lower', cmap='viridis')
    plt.show()

    #Writing to FITS file
    fits_newfile_name = filename

```

```

vhdr = hdu[0].header
print(type(cutout))

fits.writeto(fits_newfile_name,cutout.data,vhdr,overwrite=True)

return cutout.data

#making the cutout
cutout35 = hdu1010a

#picking the center
one = np.zeros((1, 2))
one[0] = [670.54499, 708.83398]

#saving to drive
filename = "/Users/iman/Documents/Midd_Coursework/Fall_2022/704/amnh/swiftuvot4/1cutout.fits"
cut1 = cutout(one[0][0], one[0][1], data11a, cutout35, filename)

#second cutout
cutout42 = hdu3010a

#picking the center
one = np.zeros((1, 2))
one[0] = [625.45402, 604.54646]

#saving to drive
filename = "/Users/iman/Documents/Midd_Coursework/Fall_2022/704/amnh/swiftuvot4/2cutout.fits"
cut2 = cutout(one[0][0], one[0][1], data22a, cutout42, filename)

### making difference image

difference = cv2.subtract(cut1, cut2)

### now saving image

hduu = fits.HDUList()
hduu.append(fits.PrimaryHDU())

#for img in export_array:
hduu.append(fits.ImageHDU(data=difference))

#giving difference image a proper header
hduu[0].header = hdu1010[0].header
hduu[1].header = hdu1010[1].header

hduu.writeto('/Users/iman/Documents/Midd_Coursework/Fall_2022/704/amnh/swiftuvot4/diff.fits',
overwrite = True)

#now, we can open the difference image in ds9 for analysis.

```

B. APPENDIX B: CANDIDATES

(Candidate list begins on next page.)

Table 2. Candidates in Pair 1

Number	R.A.	DEC
	(J2000)	(J2000)
1	21:29:51.5652	12:06:30.150
2	21:29:50.4856	12:14:08.651
3	21:29:31.5624	12:11:35.552
4	21:29:50.9979	12:19:03.071
5	21:30:11.2183	12:14:21.499
6	21:30:09.4219	12:13:40.307
7	21:30:09.2657	12:13:35.730
8	21:29:50.2179	12:10:26.933
9	21:29:56.6969	12:13:11.728
10	21:29:55.6821	12:13:07.152
11	21:29:53.1840	12:12:31.676
12	21:30:03.3319	12:12:31.661
13	21:30:00.9903	12:12:51.122
14	21:30:05.0490	12:12:13.345
15	21:30:03.9559	12:11:56.182
16	21:29:47.7200	12:11:32.163
17	21:30:09.4198	12:11:44.720
18	21:30:15.2738	12:11:35.537
19	21:30:11.6820	12:10:34.900
20	21:30:05.2819	12:10:45.224
21	21:30:13.7878	12:09:29.658
22	21:30:09.3390	12:09:14.800
23	21:30:05.9810	12:06:59.769
24	21:29:41.3209	12:09:15.966
25	21:29:59.0094	12:11:34.401
26	21:30:00.9515	12:11:01.283
27	21:30:01.0869	12:10:48.037
28	21:30:03.2549	12:10:36.773
29	21:30:02.3056	12:09:34.521
30	21:30:02.8476	12:09:33.195
31	21:30:06.8676	12:09:49.078
32	21:30:00.9503	12:08:58.761
33	21:30:00.8598	12:08:39.554
34	21:29:59.0984	12:08:37.571
35	21:29:56.5694	12:08:46.846
36	21:29:56.2984	12:08:43.535
37	21:29:53.4079	12:08:33.603
38	21:29:54.5371	12:09:10.028
39	21:29:55.0340	12:09:39.830
40	21:29:55.5760	12:09:36.518
41	21:29:50.9238	12:10:24.867
42	21:29:46.4975	12:10:09.631

Table 3. Candidates in Pair 2

Number	R.A.	DEC
	(J2000)	(J2000)
43	21:30:13.6223	12:09:23.689
44	21:30:01.2782	12:09:44.315
45	21:30:00.7058	12:09:50.990
46	21:30:00.1855	12:09:43.359
47	21:29:59.2101	12:09:23.330
48	21:29:55.3726	12:09:42.396
49	21:29:53.6820	12:09:14.734
50	21:29:52.3808	12:09:47.156
51	21:29:50.8848	12:09:47.150
52	21:29:50.0387	12:10:21.480
53	21:30:03.3075	12:09:03.308
54	21:30:06.8195	12:08:51.865
55	21:30:11.2422	12:09:37.640
56	21:30:09.2259	12:09:09.985
57	21:30:12.6076	12:08:35.649
58	21:30:04.0235	12:05:43.033
59	21:30:03.9585	12:05:43.033
60	21:30:03.7636	12:04:54.395
61	21:29:58.6266	12:05:49.702
62	21:30:03.3720	12:11:39.713
63	21:30:03.3070	12:11:39.713
64	21:30:03.8273	12:11:47.343
65	21:30:09.2913	12:11:40.668
66	21:30:00.7697	12:12:46.469
67	21:30:09.0964	12:13:30.342
68	21:30:09.2916	12:13:35.111
69	21:29:50.2951	12:14:02.737
70	21:30:01.4590	12:10:33.542
71	21:29:57.9811	12:10:33.536
72	21:29:53.2383	12:10:38.160

Table 4. Candidates in Pair 3

Number	R.A.	DEC
	(J2000)	(J2000)
73	21:30:19.5226	12:09:53.601
74	21:30:00.8723	12:14:24.216
75	21:30:00.3107	12:15:32.882
76	21:29:51.1292	12:14:06.369
77	21:30:07.0533	12:11:55.882
78	21:30:00.4025	12:11:18.819
79	21:29:47.1960	12:10:06.035
80	21:29:45.6038	12:10:12.899
81	21:29:54.2204	12:09:20.719
82	21:29:50.8489	12:09:01.492
83	21:29:47.9457	12:08:45.010
84	21:30:10.1415	12:09:12.447
85	21:30:03.8663	12:08:40.880
86	21:29:59.4643	12:07:33.596
87	21:29:51.5984	12:05:51.975
88	21:29:53.3774	12:05:01.162
89	21:30:04.6129	12:04:58.401
90	21:29:52.6283	12:08:10.680
91	21:29:54.2203	12:08:09.307
92	21:29:56.5779	12:10:27.336
93	21:30:10.6262	12:09:41.525
94	21:30:04.5136	12:11:15.007
95	21:29:51.3098	12:07:16.598

Table 5. Candidates in Pair 4

Number	R.A.	DEC
	(J2000)	(J2000)
96	21:30:00.1378	12:15:36.850
97	21:29:51.3683	12:14:58.954
98	21:29:50.9186	12:14:09.515
99	21:30:05.5315	12:12:15.783
100	21:30:04.8573	12:12:33.913
101	21:30:01.3729	12:12:53.698
102	21:30:02.6082	12:11:03.280
103	21:30:02.1586	12:11:04.929
104	21:30:02.4957	12:10:55.040
105	21:30:00.3604	12:11:23.061
106	21:30:02.0459	12:10:38.562
107	21:29:53.9536	12:11:37.900
108	21:29:46.9849	12:11:18.122
109	21:29:46.9852	12:10:10.555
110	21:30:02.6075	12:10:07.249
111	21:30:03.2815	12:09:35.935
112	21:30:03.8431	12:09:11.214
113	21:30:10.4744	12:09:44.151
114	21:30:11.8231	12:09:45.793
115	21:30:14.1829	12:09:30.950
116	21:30:16.5424	12:09:06.218
117	21:30:19.3534	12:09:57.289
118	21:29:58.1122	12:10:53.401
119	21:29:56.9876	12:08:48.155
120	21:29:56.8752	12:08:44.860
121	21:29:54.0656	12:08:13.550
122	21:29:51.0315	12:07:20.815
123	21:29:56.4253	12:07:22.461
124	21:29:59.2347	12:07:38.937
125	21:30:00.1339	12:08:02.007
126	21:30:00.4702	12:06:29.720
127	21:30:04.4018	12:05:02.368
128	21:30:11.1430	12:04:55.752
129	21:29:44.7379	12:09:04.632
130	21:29:36.1966	12:09:16.146
131	21:29:41.7057	12:05:45.221
132	21:30:09.5740	12:08:34.940
133	21:29:53.9535	12:10:40.221
134	21:29:52.8295	12:09:55.725
135	21:29:51.3685	12:09:59.021
136	21:29:51.5933	12:09:27.710
137	21:30:04.6272	12:05:50.159

Table 6. Candidates in Pair 5

Number	R.A.	DEC
	(J2000)	(J2000)
138	21:29:51.9747	12:09:50.372
139	21:29:52.1995	12:09:45.428
140	21:29:50.6260	12:09:52.016
141	21:29:49.7264	12:10:24.973
142	21:29:51.6388	12:08:09.844
143	21:29:46.1302	12:10:03.536
144	21:29:51.0783	12:06:27.668
145	21:29:52.9878	12:07:33.592
146	21:29:59.7300	12:07:55.028
147	21:30:03.5509	12:04:57.048
148	21:30:06.9221	12:08:03.269
149	21:29:55.6849	12:07:13.822
150	21:29:54.3336	12:11:47.384
151	21:30:01.8645	12:12:30.242
152	21:30:09.0583	12:11:42.449
153	21:30:10.7454	12:14:17.356
154	21:30:11.7522	12:03:44.531
155	21:29:55.8226	12:10:30.105
156	21:29:58.3969	12:11:14.482
157	21:29:59.1197	12:10:54.615
158	21:30:00.4751	12:09:55.010
159	21:29:56.5908	12:09:43.746
160	21:30:06.4371	12:10:03.621
161	21:30:09.5535	12:09:41.763
162	21:30:10.9536	12:09:41.099
163	21:30:13.3473	12:09:26.524
164	21:29:52.9769	12:10:40.033
165	21:29:57.9907	12:10:28.122
166	21:30:03.0946	12:11:42.302
167	21:30:02.5075	12:10:07.595
168	21:29:57.4945	12:08:52.090
169	21:29:54.1071	12:09:05.991